Chapter 7
Optical Coherence Tomography: A Concept Review

Pedro Serranho, António Miguel Morgado and Rui Bernardes

Abstract Optical coherence tomography (OCT) is an imaging modality broadly used in biological tissue imaging. In this chapter, we review the history of OCT and its development throughout the last years. We will focus on the physical concept of OCT imaging of the eye fundus, considering several settings currently used. We also list some research directions of recent and ongoing work concerned with the future developments of the technique and its application.

7.1 Introduction

Optical coherence tomography (OCT) is a useful and common technique in ophthalmologic imaging. This technique allows to obtain a 3D representation of the eye fundus based on the different reflectivity from the different retinal layers. For clinical evaluation purposes, one gets a series of parallel 2D cross-section representations of the eye fundus. OCT image quality and resolution gave it the nickname of optical biopsy in some literature. It allows an axial resolution of 1–15 μm (e.g., [1,2]) in images of biological tissue obtained in situ and in real time. This is clearly an advantage in cases where standard excisional biopsy carries high risks or is not possible, as in the case of the human retina, therefore the popularity of OCT for human ocular fundus imaging. Previous axial ocular imaging techniques (along the depth axis) were based in ultrasound, e.g., [3]. However, OCT superior axial resolution (about one order of magnitude in comparison with ultrasound, which lies about 200 μm [4]) gives the clinician structural information of the retina

P. Serranho (✉)
Department of Science and Technology, Open University, Campus TagusPark, Av. Dr. Jacques Delors, 2740-122 Porto Salvo, Oeiras, Portugal

IBILI-Institute for Biomedical Research in Light and Image, Faculty of Medicine, University of Coimbra, Portugal
e-mail: pserranho@uab.pt

R. Bernardes and J. Cunha-Vaz (eds.), *Optical Coherence Tomography*,
Biological and Medical Physics, Biomedical Engineering,
DOI 10.1007/978-3-642-27410-7_7,

and its layers at a biopsy level. Moreover, OCT is a noncontact technique, which is a huge benefit in eye imaging in terms of patients' comfort during the examination, on top of not needing anesthesia.

Highly transparent tissues such as the retina can be imaged by OCT. The little backscattering of light occurring in the retinal highly transparent tissue is recovered by light interferometry, which is the physical principle behind OCT. While ultrasound is based on sound waves echo delay measurements, OCT techniques use interferometry to measure the optical path of backscattered light.

Another important aspect of OCT is that the axial or depth resolution of the system is almost totally independent from the lateral resolution. The axial resolution depends mainly on the coherence properties of the light source, namely, the length of coherence as we will detail further ahead in (7.3). For ultrahigh-resolution OCT, the axial resolution is about 1 μm for nontransparent tissue [5]. This technique was later applied in ophthalmic imaging with axial resolution of 2–3 μm [6, 7]. As for the lateral resolution, it depends on the optical quality of the optical system, including the patient's eye, being constrained by the pupil size and the system optical aberrations. For retinal imaging, transverse resolution is approximately 15 μm in every retinal OCT image obtained in an axial signal acquisition setting [6]. This lateral resolution can be improved by a full-field OCT (FF-OCT) setting as we will detail in the respective section further ahead or using adaptive optics, as discussed in detail in another chapter of the book (Chap. 10).

To obtain higher axial resolution in OCT, infrared broad bandwidth light sources are advised in order to get the required low-coherence length [as detailed in (7.3) further ahead]. However, the central wavelength for retinal imaging needs to be around 800 nm. Otherwise, due to its aqueous nature, the humor vitreous would highly absorb the light. Therefore, retinal imaging OCT is restricted in terms of bandwidth of the light source. Nonetheless, it allows unprecedented axial resolution of retinal tissue in comparison to other techniques.

Actual trends in OCT research and recent work comprehend obtaining functional information from OCT data [8–10]. These works are anchored on the fact that many diseases affect local optical properties of the retina and therefore changes of these properties should be encoded in backscattered light data gathered by OCT. Another research direction currently under consideration is to adapt incident light properties in order to image the choroid [11, 12], since at wavelengths around 800 nm, this is not possible. Imaging with 1,040–1,060 nm center wavelengths results in deeper penetration into the retina. However, water absorption limits the usable bandwidth at these wavelengths, when compared to the available bandwidth at 800 nm, leading to worse axial resolution. Adaptive optics for improving transverse resolution and polarization sensing for early detection of structural changes in retinal tissues, through birefringence assessment, are two other active research areas in ophthalmological OCT.

In this review, we intend to give a comprehensive yet accurate insight of the OCT technical formulation and concept, focusing on its application on eye fundus imaging. We will describe the early years of the technique and its development until recent years. We will also describe the main physical principles behind OCT imaging, both in the time-domain and in the frequency-domain approaches, giving

a comprehensive insight on the physical concept that allows to attain structural information from backscattering of low-coherence light. In the last section, we will focus on the latest developments in the technique and in future directions aimed by several research groups.

Though OCT is a recent topic, several review papers on OCT are available. Apart from the reviews [2, 13–17] covering the OCT theory and applications as a whole, we refer to [18] for a technical review on the principles and applications of OCT, to [19] for OCT in nontransparent tissue, to [20] for the development of OCT as a clinical tool, to [21, 22] for a review on OCT as a fast nondestructive testing modality, and to [23, 24] for more recent reviews on spectral-domain OCT (SD-OCT).

7.2 The Genesis of OCT

The optical concept behind OCT, based on low-coherence interferometry, is similar to the one used about 40 years ago in [25] for thin film thickness measurement. However, most of the denominations (e.g., A-scan, B-scan, and C-scan) in OCT are borrowed from ultrasound imaging. In a hand-waiving way, while in ultrasonography depth information is obtained directly by measuring sound echo times, OCT retrieves depth through low-coherence interference between backscattered light and a reference beam. The first biomedical application of the backscattering light interferometry principle using partially coherent light was for the measurement of the length of the eye [26]. Two years later, the first approach for cross-sectional eye fundus imaging using time-domain (TD) low-coherence interferometry was presented at the ICO-15 SAT [27] and later published in [28] using the laser Doppler principle. In the latter, a 1D profile of the retinal pigment epithelium (RPE) of the human eye was obtained in vivo. This technique appeared as a higher-resolution alternative for previous developed clinical techniques based on ultrasonic echo-impulse techniques [3] that were standard for about 30 years. Among the disadvantages of the ultrasound technique [3] in comparison to low-coherence light interferometry [28] are the need for mechanical contact between the apparatus and the eye (therefore requiring anesthesia) and poorer axial resolution.

OCT as a technique for eye fundus volumetric imaging is anchored in the work by the group of Fujimoto in 1991 [29], where lateral scanning was introduced to the system and a fiber optic Michelson interferometer was used for time-domain low-coherence light interferometry. In vivo 2D tomograms were published 2 years later by Fercher et al. [30] and Swanson et al. [31]. Several studies regarding the properties of OCT were presented in the following years, regarding, for instance, its statistics of attenuation and backscattering [32] and its resolution for the anterior segment [33]. The validation of OCT for human eye fundus imaging was established in [34], in the sense that a correlation was found between OCT results and the known anatomy of the eye. In [35], 3D OCT images are reported, with an acquisition time of 20 s for the 40 frames of the volumetric data, which was prone to errors

due to saccades. In [36], 3D scans (64 × 256 × 128 voxels) of the human retina were obtained in 1.2 s by the conjugation of the transverse scanning approach of confocal scanning and the depth scanning capability of OCT, making it possible to obtain OCT volumes of the human retina with minor movement errors due to the substantial reduction of the acquisition time.

Another important development was to consider the interferometry phenomena in the spectral domain, also called Fourier or frequency domain. Two ways were considered to this end. The first uses a spectrometer to measure the interferometric signal in the Fourier domain. The second employs a tunable light source that would sweep the frequency range of interest. This development allowed higher resolution of the obtained volumetric data and lower acquisition time (since the reference arm was kept fix). In a way, all the backscattering effect for each A-scan is measured simultaneously instead of moving the reference mirror to measure the backscattering light for each depth distance. The work of Fercher et al. [37] used backscattering spectral interferometry for the measurement of intraocular distances, both on a model eye and in vivo human eye. As in the first approaches in time-domain interferometry, the latter originated a 1D reflectivity profile of the human eye fundus. The work of [38] introduced a new concept for SD-OCT by considering source frequency tuning, which decreased acquisition time. Following the same principle, in [39], the in vivo acquisition time was in the order of the millisecond, and several intraocular distances were obtained simultaneously in a 1D profile. In [40], the frequency range (1,200–1,275 nm) is swept by a tunable laser in less than half the time, that is, 500 μs, allowing a scan rate of 2 kHz and an axial resolution of 15 μm. Häusler et al. [41] used the frequency-domain OCT concept for skin imaging.

Though the faster acquisition time was clear since the arrival of the Fourier domain OCT in 1995, only in 2003 [42–44] the sensitivity of time and Fourier domain setups is compared, being the performance of the latter clearly better. This was then extended to the comparison of macular thickness measurements [45] and implications on the measurement of macular edema [46]. Moreover, the first in vivo 2D tomogram of the human retina using SD-OCT was only published in 2002 [47], followed by the 3D retinal imaging in 2005 [7].

Several developments have been considered and suggested in the OCT technique and instrumentation in order to improve the results. Among these are attempts to increase depth and axial resolution and good choices of appropriate emission wavelength for choroid imaging. Several postprocessing methods for OCT images were also carried out more recently. We will refer to recent developments and future directions concerning OCT imaging in the last section of this chapter.

7.3 The Physical Principle

As already mentioned, OCT physical principle is similar to ultrasound imaging, using light instead of sound wave propagation and reflection. Ultrasound imaging is based on echo times, that is, it takes into account the time that an emitted sound

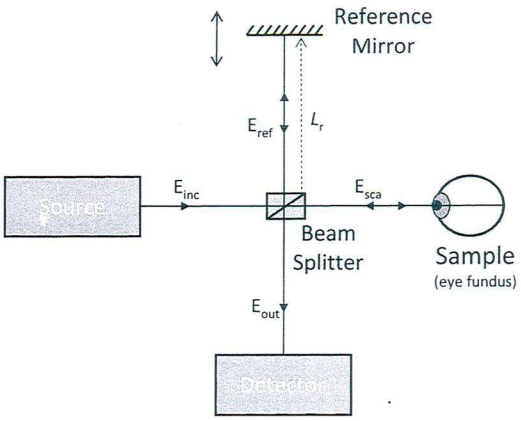

Fig. 7.1 Scheme for the principle of time-domain optical coherence tomography

signal takes to echo back from the structure to be imaged, usually called the sample. In OCT, as light travels much faster than sound, physicists had to adapt the principle in order to attain the backscattering optical path, since there is no available hardware to accurately measure the time of flight for the short values imposed by the axial resolution requirement (10^{-14} s). Therefore, low-coherence light and interferometry were considered to overcome this difficulty, finding a way to measure the differences in optical path of the detected backscattered light similarly to the sound echo time that ultrasound uses for image reconstruction.

Optical interferometry is based on the interference of two light beams. One knows that when a second wave interferes with a first one, having the same frequency (i.e., the same wavelength), their interference produces a higher intensity signal if in phase, while the signal vanishes if in opposite phase. Two light beams obtained by division of a single beam are initially in phase. If these beams are mixed after traveling some distance, the interference signal will be amplified only if the beams are still in phase. That only happens if both have traveled the same optical path (the optical path is the product of the geometrical path by the medium refractive index) or if the optical path difference is an integer multiple of their wavelength. This is only true for monochromatic (i.e., single wavelength) light beams. For high-bandwidth low-coherence light, signal amplification by interference can only happen when the optical paths differ by no more than a small value, equal to the coherence length of the light source.

The use of interferometry comes now in play in OCT, in the sense that it allows to detect the distance traveled by the backscattered light (or to be more rigorous, its optical path) in the following way (see Fig. 7.1): an incident low-coherence beam of light is split in two by a beam splitter; one of the beams travels (through a so-called sample path) to the sample and is partially backscattered, while the second beam travels (through a so-called reference path) to a reference mirror with a given adjustable distance to the splitter where it is also backscattered. The two backscattered beams are then again recombined, and the interference is measured. If the interference signal is high, it means that a lot of backscattered light from

the sample comes from the same optical path distance of the reference mirror. The position of the mirror is ranged in the imaging depth range of interest in order to get a full A-scan profile. In this way, one gets a map of reflectivity of the sample along an axial depth direction. This rationale is the basis for time-domain OCT (TD-OCT).

7.4 Low-Coherence Light Interferometer

As already mentioned, the scheme for the principle of OCT imaging is presented in Fig. 7.1.

Low-coherence light is the superposition of a finite bandwidth of frequencies, so the incident field reaching the beam splitter can be characterized by

$$E_{\text{inc}}(\omega, t) = A(\omega)\mathrm{e}^{-\mathrm{i}\omega t},$$

where i is the complex unit, ω is the frequency, and $A(\omega)$ is the correspondent amplitude spectrum of the source field. Since the initial phase of the incident wave is arbitrary, we have let it drop for the sake of simplicity [16]. In the beam splitter, the incident beam is divided in the reference incident beam with amplitude $A_{\text{r}}(\omega)$ and the sample incident beam with amplitude $A_{\text{s}}(\omega)$ with $A_{\text{r}}(\omega) + A_{\text{s}}(\omega) \leq 1$. The backscattered fields at the interferometer from the reference mirror and sample arm are therefore given by

$$E_{\text{ref}}(\omega, t, L_{\text{r}}) = A_{\text{r}}(\omega)\mathrm{e}^{-\mathrm{i}(2\beta_{\text{r}}(\omega)L_{\text{r}}-\omega t)} \quad E_{\text{sca}}(\omega, t) = \int_0^{+\infty} A_{\text{s}}(\omega, z)\mathrm{e}^{-\mathrm{i}(2\beta_{\text{s}}(\omega,z)z-\omega t)}\mathrm{d}z,$$

where β_{r} and β_{s} are the propagating coefficients for the reference and sample paths, respectively [48]. While the coefficient β_{r} for the reference arm (air) is considered to be independent from the depth variable z in this analysis, the sample arm propagation coefficient may vary in depth within the range of transparent ocular media and air. We now consider the output beam as

$$E_{\text{out}}(\omega, t) = E_{\text{ref}}(\omega, t) + E_{\text{sca}}(\omega, t),$$

with intensity

$$J(\omega, L_{\text{r}}) = \langle E_{\text{out}} {E_{\text{out}}}^* \rangle = |A_{\text{r}}(\omega)|^2 + \left| \int_0^{+\infty} A_{\text{s}}(\omega, z)\mathrm{e}^{-2\mathrm{i}\beta_{\text{s}}(\omega,z)z}\mathrm{d}z \right|^2 + 2I(\omega, L_{\text{r}}), \tag{7.1}$$

where $\langle \cdot \rangle$ represents a time average, that is,

$$\langle f \rangle = \lim_{T \to +\infty} \frac{1}{2T} \int_{-T}^{T} f(t)\mathrm{d}t,$$

the operator * represents the complex conjugate, L_r is the distance to the position of the reference mirror, and $I(\omega, L_r)$ is the real part of the so-called cross-interference. We point out that the two first terms of the intensity of the beam in (7.1) do not depend on the position of the reference mirror and are therefore called the self-interference. The cross-interference is therefore the important term for OCT image reconstruction and is proportional to [16]

$$I(\omega, L_r) \propto Re(\langle E_{ref} E_{sca}{}^* \rangle).$$

In this way, the cross-interference may be written as [48]

$$I(\omega, L_r) \propto \int_0^{+\infty} \tilde{I}(\omega, z)\mathrm{d}z, \tag{7.2}$$

where $\tilde{I}(\omega, z)$ is the cross-interference contribution from the reflectivity in the sample from distance z given by

$$\tilde{I}(\omega, z) = Re\left(A_r(\omega) A_s(\omega, z)^* \mathrm{e}^{-2\mathrm{i}\Delta\theta(\omega, z)}\right),$$

with each phase half mismatch for each backscattering distance given by

$$\Delta\theta(\omega, z) = \beta_r(\omega) L_r - \beta_s(\omega, z) z.$$

In the previous analysis, we did not yet refer to the low coherence of light sustaining the OCT principle. In fact, the low-coherence property comes from the fact that light source has several frequencies. In mathematical terms, the detected intensity is not given by (7.2) but by its integral over the range of frequencies of the light source. This integral defines the coherence length, since the periodic term of the complex exponential disappears by the integration over the frequency variable. The higher the bandwidth considered in the source, the lower the length of coherence.

For a Gaussian spectrum (i.e., a Gaussian-like distribution of frequencies), the length of coherence is given by [18]

$$l_C = \frac{4 \ln 2}{\pi} \frac{\bar{\lambda}^2}{\Delta\lambda}, \tag{7.3}$$

where $\bar{\lambda}$ is the central wavelength and $\Delta\lambda$ is the spectral width. The axial resolution is given by half of the length of coherence [16]. It is clear that the resolution improves if the bandwidth $\Delta\lambda$ is higher and the mean wavelength $\bar{\lambda}$ is lower, suggesting the use of broad bandwidth light source. However, depending on the imaging application, these values have additional constraints. In nontransparent tissue like skin, wavelengths centered at about 1,300 nm are used to obtain better penetration, namely, about 2–3 mm [2, 19], with bandwidths ranging from 300 to 800 nm. However, for eye imaging, these wavelengths cannot be used due to water absorption in the ocular media [6]. For instance, usual OCT machines

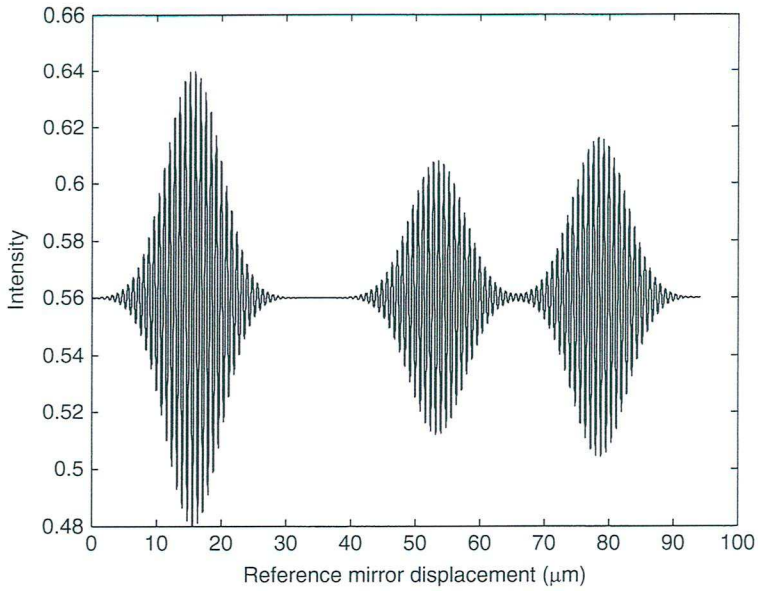

Fig. 7.2 Computer-simulated example of interference occurring at 16-, 53-, and 79-μm depth distances in the reference arm

consider values similar to $\bar{\lambda} = 820\,\text{nm}$ and $\Delta\lambda = 20\,\text{nm}$, therefore allowing an axial resolution of about 15 μm [18]. In [16], a setting with $\bar{\lambda} = 800\,\text{nm}$ and $\Delta\lambda = 50\,\text{nm}$ is considered, which corresponds to an axial resolution of approximately 6 μm. Ultrahigh-resolution OCT considers $\bar{\lambda} = 800\,\text{nm}$ and $\Delta\lambda = 350\,\text{nm}$, allowing an axial resolution below 1 μm [6].

We note that the coherence length determines the spatial length of interest within the sample around each considered reference arm length L_r. In this way, only backscattered light from within this range in the sample arm contributes to interference with the reference beam. An illustration of interference between the reference and sample beam is shown in Fig. 7.2.

7.5 Time-Domain Optical Coherence Tomography

For TD-OCT, the detector measures the sum of the intensities at each considered frequency. Therefore, from (7.1), one gets, for each position considered for the reference mirror at distance L_r, the intensity

$$J(L_r) = \int_{-\infty}^{+\infty} \left(|A_r(\omega)|^2 + \left| \int_0^{+\infty} A_s(\omega, z) e^{-2i\beta_s(\omega)z} dz \right|^2 + 2I(\omega, L_r) \right) d\omega.$$

In this way, one gets a map of interferometry in depth related to the optical properties that gives information on the intensity of backscattered light from each optical path distance considered. This correlates with structural data of the sample (e.g., [34]). Instrumentation techniques are used to obtain only the cross-interference term, namely, by considering appropriate constant velocities for the movement of the reference mirror that facilitate the removal of the background self-interference (e.g., [13]).

7.6 Spectral-Domain Optical Coherence Tomography

Spectral or Fourier domain OCT also relies on interferometry, but the measurements are taken in the frequency space. In fact, in the physical setting, the detector is replaced by a spectrometer to this end. Therefore, one of the main advantages in this approach is that the reference mirror is kept fixed allowing a faster acquisition time, since no moving parts exist.

In the context of SD-OCT, one looks at (7.1) in terms of frequency for a given fixed L_r. At the receiving spectrometer, one gets the intensity spectrum given by (7.1) with respect to a frequency ω. In order to obtain the depth information in the time domain, a Fourier transform is performed, that is,

$$J(t) = \hat{J}(\omega),$$

where the hat $\wedge$ holds for Fourier transform. For faster computation, usually fast Fourier transform (FFT) is considered, since the intensity spectrum $J(\omega)$ is measured at equally spaced discrete frequency values, that is, one recovers a discrete set of intensities corresponding to a set of equally spaced frequency values. If one considers N data points in the frequency domain, the result after FFT consists of $N/2$ points in the time domain. The time resolution is given by

$$\Delta t = \frac{1}{c}\frac{\bar{\lambda}^2}{\Delta\lambda},$$

where $\bar{\lambda}$ and $\Delta\lambda$ are defined as in (7.3) and c is the speed of light [16]. A spatial step is obtained by multiplying the previous equation by the speed of light in the medium, that is,

$$\Delta z = \frac{1}{n_s}\frac{\bar{\lambda}^2}{\Delta\lambda},$$

where n_s is the constant refractive index in the sample arm. If one considers a detector array of N elements in the frequency domain, the maximum depth is given by

$$z_{\max} = \frac{N}{4n_s}\frac{\bar{\lambda}^2}{\Delta\lambda},$$

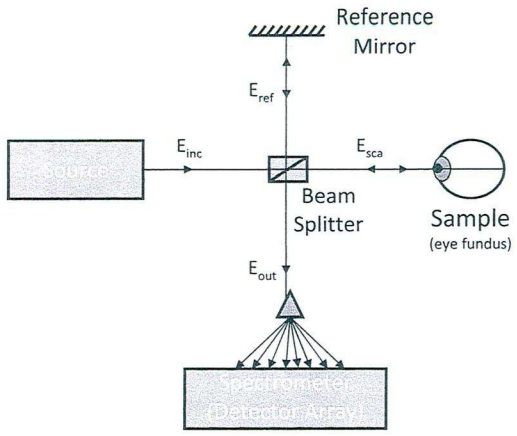

Fig. 7.3 Scheme for the principle of spectral-domain optical coherence tomography

where a division by 2 is needed in order to account for the travel through the sample arm in both directions. In an aqueous medium with $n_s = 1.33$, and considering $\bar{\lambda} = 800\,\text{nm}$ and $\Delta\lambda = 50\,\text{nm}$ as before and $N = 1,024$ elements in the detector, one gets $z_{\max} \approx 2.46\,\text{mm}$. For air with $n_s = 1.0008$, we get $z_{\max} \approx 3.27\,\text{mm}$. However, considering $\bar{\lambda} = 820\,\text{nm}$ and $\Delta\lambda = 20\,\text{nm}$, one gets maximum depths for water and air of $z_{\max} \approx 6.47\,\text{mm}$ and $z_{\max} \approx 8.54\,\text{mm}$, respectively. Therefore, one can only aim for information within this range, which for the retina is sufficient.

It is also worth mentioning that, in a spectrometer-based SD-OCT setting, the acquisition time is governed by the readout rate of the spectrometer. A major drawback of this technique is the decrease of signal level and, therefore, of sensitivity, with sample depth. This is a consequence of the convolution between the point-spread function for each wavelength, whose width increases along the detector plan, toward its edge, due to optical aberrations, and the corresponding detector pixel, whose width is finite and fixed [49]. The experimental setup is illustrated in Fig. 7.3.

7.7 Swept-Source Optical Coherence Tomography

Another possibility for Fourier domain OCT is to use a tunable light source (a tunable laser) instead of a broad bandwidth one. Though this technique is also within SD-OCT, it is usually named swept-source (SS-OCT).

For each axial direction, the frequency range of interest is rapidly swept through equally spaced frequency values. This equal spacement is necessary to allow the use of fast Fourier transform. This way, instead of using a broadband light and a spectrometer to gather information on the array of frequencies considered, in SS-OCT, only one photodetector is needed. The instrumentation process at the receptor side is simplified but that is balanced by the additional need of fast sweeping tunable lasers at the source side. One advantage of SS-OCT over SD-OCT

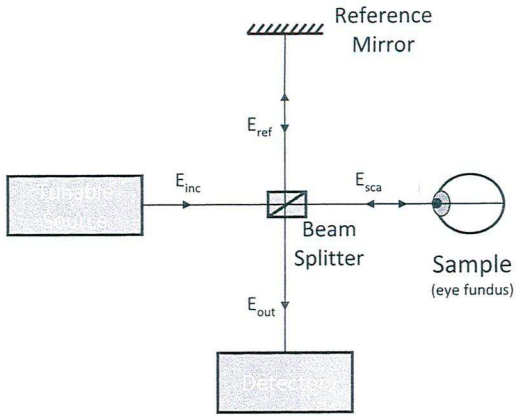

Fig. 7.4 Scheme for the principle of swept-source optical coherence tomography

is the minimal signal drop-off with depth that arises from using the same detector for all frequencies.

It is clear that the speed of acquisition of this setting is governed by the sweep speed of the laser. Several appropriate lasers to achieve this aim were developed and tested, for instance, in [39, 40, 50]. In fact, the development of tunable lasers with fast sweeping times in the range of frequencies of interest allowed to improve the acquisition time. Recent ultrahigh-speed OCT techniques were published by [51] for human retina imaging and by [52] using a Doppler OCT technique to image and quantitatively assess the retinal blood flow.

Choma and coworkers [42] compared the sensitivity of SD- and SS-OCT vs. TD-OCT. They found that TD-OCT has lower sensitivity, but the sensitivities of standard spectrometer-based SD- and SS-OCT are similar.

The development of ultrahigh-speed SS-OCT also allowed in vivo imaging of larger areas of the human retina. Actual acquisition times allow OCT imaging covering 70° field of view of 1,900 × 1,900 A-scans under 2 s [53], using this technique. The experimental setup is illustrated in Fig. 7.4.

7.8 Polarization-Sensitive Optical Coherence Tomography

Polarization-sensitive OCT (PS-OCT) gathers polarization information on top of the intensity of backscattered light. In this way, instead of recovering a scalar value of the intensity of the backscattered electromagnetic field, the measurement of polarization accounts for birefringence effects within the sample. Birefringence occurs when a medium has different refractive indexes for the two orthogonal plans of polarization. PS-OCT retrieves depth correlation information based on the birefringence within the sample.

This book has a full chapter dedicated to this modality of OCT, so we refer to Chap. 9 for more details.

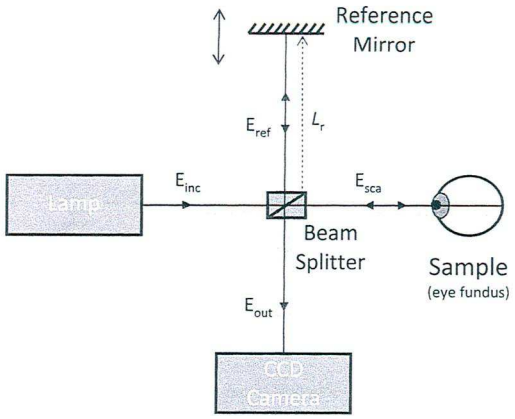

Fig. 7.5 Scheme for the principle of full-field optical coherence tomography

7.9 Full-Field Optical Coherence Tomography

FF-OCT takes advantages of both time- and spectral-domain approaches. It is based on the time-domain approach, namely, the reference mirror is shifted during acquisition time, but the acquisition time is much lower, competing with spectral-domain acquisition time. This is due to the fact that FF-OCT acquires enface images at once. Instead of acquiring information from an axial direction as both TD- and SD-OCT do, FF-OCT acquires backscattering data from the same (optical path) depth simultaneously. Therefore, though one needs the reference mirror to be moved in the spirit of TD-OCT, one does not need to move the incident light source in lateral directions over the sample.

The enface image data is acquired through the use of a charge-coupled device (CCD) camera instead of a single detector. The CCD camera captures the two-dimensional enface data from a single exposure from a thermal lamp light source instead of an axial oriented beam source. Thermal lamps are a good choice due to their relatively low price and low spatial coherence [16]. Moreover, this approach allows to improve lateral resolution. Reported axial and lateral resolutions are of 0.9 and 1.8 μm, respectively, [54] with an image time of 4 s and sensitivity of 90 dB. On the same year [55], both values of axial and lateral resolution were reduced for <1 μm, with an image acquisition time of 1 s and sensitivity of 80 dB. Later, the same principle was adapted for spectroscopic OCT [56]. It is clear that the lateral resolution of these apparatus improved significantly in comparison with the axial OCT setting, which is limited to 15 μm [6] due to the numerical aperture of the pupil. Moreover, this high-resolution performance in such short amount of time opens the path for in vivo subcellular level imaging in the future. The experimental setup is illustrated in Fig. 7.5.

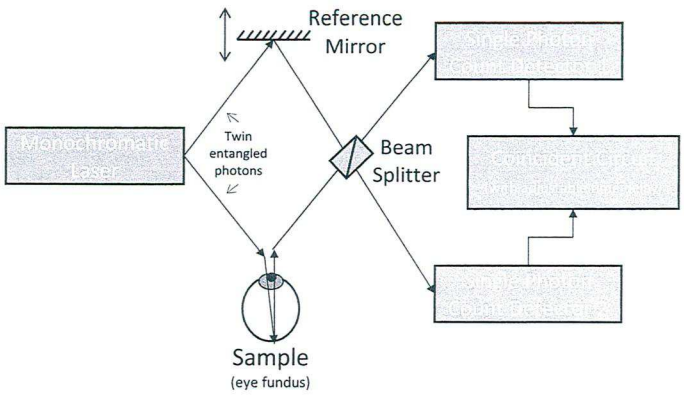

Fig. 7.6 Scheme for the principle of quantum optical coherence tomography

7.10 Quantum Optical Coherence Tomography

The axial resolution of both TD- and SD-OCT is based on the coherence length (7.3) considered. However, a new approach has been considered that promises an enhancement of twice the axial resolution as a by-product. The main difference is to take advantage of the quantum nature of light instead of its harmonic classical behavior.

Quantum OCT (Q-OCT) takes advantage of quantum light sources which light state is known. In particular, the concept takes advantage of entangled photon emission and in the principle based on the work of Hong et al. [57] that the detection probability amplitudes of an entangled state interfere destructively if two paths are equal in a properly adapted interferometer. While in classical interferometry, the interference from the same optical path distance is constructive (see Fig. 7.2), in Q-OCT, the opposite occurs. Only more recently this principle has been used in OCT [58, 59]. While dispersion of light in classical OCT originates degradation of axial resolution that needs to be overcome through numerical [60] or experimental [61] methods, quantum interference of an entangled state allows a twice axial resolution enhancement, since it is immune to dispersion. However, this needs to rely on highly efficient entangled state sources and detectors. Several works were developed subsequently to improve Q-OCT. For instance, Carrasco et al. [62] suggested improving axial resolution by chirped quasi-phase matching. The work of Nasr et al. [63] considered dispersion-canceled and dispersion-sensitive approaches in Q-OCT, in order to improve axial resolution and penetration depth. For more details on the physical principle of Q-OCT, we refer to the reviews [16, 64, 65].

Developments to consider polarization in Q-OCT were also achieved [66]. In this way, advantages of PS-OCT were added to standard Q-OCT quantum-polarized. Being immune to dispersion, polarized sensitive quantum OCT can be used to image tissue deeper than usual OCT. Details on the experimental setup can be seen in [67]. The experimental setup is illustrated in Fig. 7.6.

7.11 Latest Developments and Future Directions

OCT is a very promising imaging technique in ophthalmology due to its noninvasiveness and high-resolution characteristics. Being about 2 decades old in what concerns ophthalmology applications, research in OCT has nowadays various fronts and interests.

For instance, Bilenca et al. [68] measured the information gathered by OCT in comparison with the total information to characterize the sample in terms of Shannon information. In this way, these authors established the Shannon information limits of OCT and compared it with the current level of information that is gathered by actual OCT apparatus. The paper shows results depending on the length of coherence of light and speckle noise formation.

Another new direction of research is to use OCT data to acquire functional information of the retina status. Until recently, OCT was used to recover the internal structure of the retina, namely, information on the thickness of the whole retina or some of its layers as, for instance, the retinal nerve fiber layer. However, a new paradigm in the way researchers consider OCT data was introduced, based on the fact that it gathers information on the optical properties of the retina. Therefore, if some disease condition affects these optical properties, then OCT data should reflect these changes from the healthy state. In [8], alterations in OCT instrumentation were suggested to gather functional information on the photoreceptors from OCT data. Bernardes et al. [69] introduced the proof of concept that alterations on the blood–retinal barrier affect standard OCT data, namely, the histogram of intensities. Supposedly, leakage due to the malfunction of the blood–retinal barrier changes the refractive index of the retinal medium and therefore affects OCT data. This hypothesis is compatible with the fact that histogram changes are more stressed in upper retinal layers, where blood vessels lay. This was the purpose of a recent study by the same group [10]. In between, Grzywacz et al. [9] characterized the statistical properties of OCT data from the human retina and suggest that methods considering changes in this characterization might be used to distinguish between healthy and disease states. This characterization was also used to train an algorithm based on support vector machines (SVM) to automatically distinguish between OCT data from healthy, early stage diabetic retinopathy or macular edema diabetic retinopathy patients [70]. Accuracy by a leave-one-out cross-validation method was about 68%, which is promising in terms of allowing future automatic classification from OCT data of these three conditions. More details on these methods can be seen in Chap. 8.

Faster scanning techniques (mainly using SS-OCT) have also been a matter of interest recently [51, 52]. Ultrahigh-speed techniques allow to scan wider areas of the retina in vivo. For instance, in [53, 71], results with OCT scans covering 70° field of view are presented. The OCT scanning technique is based on swept-source OCT. Moreover, fundus images of such a wide field of view are provided by a postprocessing technique based on the mean intensity of the OCT signal between the RPE and the choroid [53].

Common wavelengths used in OCT to avoid absorption in the anterior segment, vitreous humor, and retinal media do not allow choroid imaging due to absorption. Therefore, an appropriate choice of the incident light source in order to allow choroid imaging has also been a matter of interest in recent developments. A source wavelength around 1,040 nm is more appropriate to this end [11]. Several techniques to use OCT to image both the retina and the choroid were developed thereafter [12, 72]. Ikuno and coworkers [73] used OCT high-penetration imaging techniques to test the reproducibility of choroidal thickness measurements and to correlate it with retinal thickness measurements.

References

1. J.G. Fujimoto, Optical coherence tomography for ultrahigh resolution *in vivo* imaging. Nat. Biotechnol. **21**(11), 1361–1367 (2003)
2. J.G. Fujimoto, Optical coherence tomography: principles and applications. Rev. Laser Eng. **31**, 635–642 (2003)
3. G.H. Mundt Jr., W.F. Hughes Jr., Ultrasonics in ocular diagnosis. Am. J. Ophthalmol. **41**(3), 488–498 (1956)
4. J.C. Bamber, M. Tristam, Diagnostic ultrasound, in *The Physics of Medical Imaging*, ed. by S. Webb (Adam Hilger, Bristol, 1988), pp. 319–388
5. W. Drexler, U. Morgner, F.X. Kärtner, C. Pitris, S.A. Boppart, X.D. Li, E.P. Ippen, J.G. Fujimoto, In vivo ultrahigh-resolution optical coherence tomography. Opt. Lett. **24**(17), 1221–1223 (1999)
6. W. Drexler, U. Morgner, R.K. Ghanta, F.X. Kärtner, J.S. Schuman, J.G. Fujimoto, Ultrahigh-resolution ophthalmic optical coherence tomography. Nat. Med. **7**(4), 502–507 (2001)
7. U. Schmidt-Erfurth, R.A. Leitgeb, S. Michels, B. Považay, S. Sacu, B. Hermann, C. Ahlers, H. Sattmann, C. Scholda, A.F. Fercher, W. Drexler, Three-dimensional ultrahigh-resolution optical coherence tomography of macular diseases. Invest. Ophthalmol. Vis. Sci. **46**(9), 3393–3402 (2005)
8. V.J. Srinivasan, Y. Chen, J.S. Duker, J.G. Fujimoto, In vivo functional imaging of intrinsic scattering changes in the human retina with high-speed ultrahigh resolution OCT. Opt. Express **17**(5), 3861–3877 (2009)
9. N. Grzywacz, J. de Juan, C. Ferrone, D. Giannini, D. Huang, G. Koch, V. Russo, O. Tan, C. Bruni, Statistics of optical coherence tomography data from human retina. IEEE Trans. Med. Imaging **29**(6), 1224–1237 (2010)
10. R. Bernardes, T. Santos, P. Serranho, C. Lobo, J. Cunha-Vaz, On invasive evaluation of retinal leakage using optical coherence tomography. Ophthalmologica **226**(2), 29–36 (2011)
11. A. Unterhuber, B. Považay, B. Hermann, H. Sattmann, A. Chavez-Pirson, W. Drexler, In vivo retinal optical coherence tomography at 1040 nm—enhanced penetration into the choroid. Opt. Express **13**(9), 3252–3258 (2005)
12. K. Kurokawa, K. Sasaki, S. Makita, M. Yamanari, B. Cense, Y. Yasuno, Simultaneous high-resolution retinal imaging and high-penetration, choroidal imaging by one-micrometer adaptive optics optical coherence tomography. Opt. Express **18**(8), 8515–8527 (2010)
13. J. Schmitt, Optical coherence tomography (OCT): a review. IEEE J. Sel. Top. Quant. Electron. **5**(4), 1205–1215 (1999)
14. W. Drexler, Ultrahigh-resolution optical coherence tomography. J. Biomed. Opt. **9**(1), 47–74 (2004)
15. A.G. Podoleanu, Optical coherence tomography. Br. J. Radiol. **78**(935), 976–988 (2005)

16. P.H. Tomlins, R.K. Wang, Theory, developments and applications of optical coherence tomography. J. Phys. D Appl. Phys. **38**(15), 2519–2535 (2005)
17. M.L. Gabriele, G. Wollstein, H. Ishikawa, L. Kagemann, J. Xu, L.S. Folio, J.S. Schuman. Optical coherence tomography: history, current status, and laboratory work. Invest. Ophthalmol. Vis. Sci. **52**(5), 2425–2436 (2011)
18. A.F. Fercher, W. Drexler, C.K. Hitzenberger, T. Lasser. Optical coherence tomography—principles and applications. Rep. Prog. Phys. **66**, 239–303 (2003)
19. M. Brezinski, J. Fujimoto, Optical coherence tomography: high-resolution imaging in nontransparent tissue. IEEE J. Sel. Top. Quant, Electron. **5**(4), 1185–1192 (1999)
20. A. Zysk, F. Nguyen, A. Oldenburg, D. Marks, S. Boppart, Optical coherence tomography: a review of clinical development from bench to bedside. J. Biomed. Opt. **12**(5), 051403 (2007)
21. M. Wurm, K. Wiesauer, K. Nagel, M. Pircher, E. Götzinger, C.K. Hitzenberger, D. Stifter, in *Spectral Domain Optical Coherence Tomography: A Novel And Fast Tool For NDT. IVth NDT in Progress*, Prague, Czech Republic, 5–7 November 2007
22. D. Stifter, K. Wiesauer, M. Wurm, E. Leiss, M. Plircher, E. Götzinger, B. Baumann, C.K. Hitzenberger, in *Advanced Optical Coherence Tomography Techniques: Novel and Fast Imaging Tools for Non-destructive Testing. 17th World Conference on Nondestructive Testing*, Shanghai, China, 25–28 October 2008
23. Z. Yaqoob, J. Wu, C. Yang, Spectral domain optical coherence tomography: a better OCT imaging strategy. BioTechniques **39**(6), 6–13 (2005)
24. S. Wolf, U. Wolf-Schnurrbusch, Spectral-domain optical coherence tomography use in macular diseases: a review. Ophthalmologica **224**(6), 333–340 (2010)
25. P.A. Flournoy, R.W. McClure, G. Wyntjes, White-light interferometric thickness gauge. Appl. Opt. **11**(9), 1907–1915 (1972)
26. A.F. Fercher, K. Mengedoht, W. Werner, Eyelength measurement by interferometry with partially coherent light. Opt. Lett. **13**(3), 186–188 (1988)
27. F. Fercher, Ophthalmic interferometry, in *Proceedings of the International Conference on Optics in Life Sciences*. ed. by G. von Bally, S. Khanna, Garmisch-Partenkirchen, Germany, 12–16 August 1990, pp. 221–228, (ISBN 0–444–89860–3)
28. C.K. Hitzenberger, Optical measurement of the axial eye length by laser Doppler interferometry. Invest. Ophthalmol. Vis. Sci. **32**(3), 616–624 (1991)
29. D. Huang, E.A. Swanson, C.P. Lin, J.S. Schuman, W.G. Stinson, W. Chang, M.R. Hee, T. Flotte, K. Gregory, C.A. Puliafito, Optical coherence tomography. Science **254**(5035), 1178–1181 (1991)
30. A.F. Fercher, C.K. Hitzenberger, W. Drexler, G. Kamp, H. Sattmann, In vivo optical coherence tomography. Am. J. Ophthalmol. **116**(1), 113–114 (1993)
31. E.A. Swanson, J.A. Izatt, M.R. Hee, D. Huang, C.P. Lin, J.S. Schuman, C.A. Puliafito, J.G. Fujimoto, In vivo retinal imaging by optical coherence tomography. Opt. Lett. **18**(21), 1864–1866 (1993)
32. J.M. Schmitt, A. Knüttel, M. Yadlowsky, M.A. Eckhaus, Optical-coherence tomography of a dense tissue: statistics of attenuation and backscattering. Phys. Med. Biol. **39**(10), 1705–1720 (1994)
33. J.A. Izatt, M.R. Hee, E.A. Swanson, C.P. Lin, D. Huang, J.S. Schuman, C.A. Puliafito, J.G. Fujimoto, Micrometer-scale resolution imaging of the anterior eye in vivo with optical coherence tomography. Arch. Ophthalmol. **112**(12), 1584–1589 (1994)
34. M.R. Hee, J.A. Izatt, E.A. Swanson, D. Huang, J.S. Schuman, C.P. Lin, C.A. Puliafito, J.G. Fujimoto, Optical coherence tomography of the human retina. Arch. Ophthalmol. **113**(3), 325–332 (1995)
35. A. Podoleanu, J. Rogers, D. Jackson, S. Dunne, Three dimensional OCT images from retina and skin. Opt. Express **7**(9), 292–298 (2000)
36. C. Hitzenberger, P. Trost, P.W. Lo, Q. Zhou, Three-dimensional imaging of the human retina by high-speed optical coherence tomography. Opt. Express **11**(21), 2753–2761 (2003)
37. A.F. Fercher, C.K. Hitzenberger, G. Kamp, S.Y. El-Zaiat, Measurement of intraocular distances by backscattering spectral interferometry. Opt. Commun. **117**, 43–48 (1995)

38. S.R. Chinn, E.A. Swanson, J.G. Fujimoto, Optical coherence tomography using a frequency-tunable optical source. Opt. Lett. **22**(5), 340–342 (1997)
39. F. Lexer, C.K. Hitzenberger, A.F. Fercher, M. Kulhavy, Wavelength-tuning interferometry of intraocular distances. Appl. Opt. **36**(25), 6548–6553 (1997)
40. B. Golubovic, B.E. Bouma, G.J. Tearney, J.G. Fujimoto, Optical frequency-domain reflectometry using rapid wavelength tuning of a Cr4+: forsterite laser. Opt. Lett. **22**(22), 1704–1706 (1997)
41. G. Häusler, M.W. Lindner, "Coherence radar" and "spectral radar"—new tools for dermatological diagnosis. J. Biomed. Opt. **3**(1), 21–31 (1998)
42. M. Choma, M. Sarunic, C. Yang, J. Izatt, Sensitivity advantage of swept source and Fourier domain optical coherence tomography. Opt. Express **11**(18), 2183–2189 (2003)
43. J.F. de Boer, B. Cense, B.H. Park, M.C. Pierce, G.J. Tearney, B.E. Bouma, Improved signal-to-noise ratio in spectral-domain compared with time-domain optical coherence tomography. Opt. Lett. **28**(21), 2067–2069 (2003)
44. R. Leitgeb, C. Hitzenberger, A. Fercher, Performance of Fourier domain vs. time domain optical coherence tomography. Opt. Express **11**(8), 889–894 (2003)
45. C.K. Leung, C.Y. Cheung, R.N. Weinreb, G. Lee, D. Lin, C.P. Pan, D.S. Lam, Comparison of macular thickness measurements between time domain and spectral domain optical coherence tomography. Invest. Ophthalmol. Vis. Sci. **49**(11), 4893–4897 (2008)
46. F. Forooghian, C. Cukras, C.B. Meyerle, E.Y. Chew, W.T. Wong, Evaluation of time domain and spectral domain optical coherence tomography in the measurement of diabetic macular edema. Invest. Ophthalmol. Vis. Sci. **49**(10), 4290–4296 (2008)
47. M. Wojtkowski, R. Leitgeb, A. Kowalczyk, T. Bajraszewski, A.F. Fercher, In vivo human retinal imaging by Fourier domain optical coherence tomography. J. Biomed. Opt. **7**(3), 457–463 (2002)
48. B.E. Bouma, G.J. Tearnley (eds.), *Handbook of Optical Coherence Tomography* (Marcel Dekker, New York, 2002)
49. Z. Hu, Y. Pan, A.M. Rollins, Analytical model of spectrometer-based two-beam spectral interferometry. Appl. Opt. **46**(35), 8499–8505 (2007)
50. M.A. Choma, K. Hsu, J.A. Izatt, Swept source optical coherence tomography using an all-fiber 1300-nm ring laser source. J. Biomed. Opt. **10**(4), 44009 (2005)
51. B. Potsaid, B. Baumann, D. Huang, S. Barry, A.E. Cable, J.S. Schuman, J.S. Duker, J.G. Fujimoto, Ultrahigh speed 1050 nm swept source/Fourier domain OCT retinal and anterior segment imaging at 100,000 to 400,000 axial scans per second. Opt. Express **18**(19), 20029–20048 (2010)
52. B. Baumann, B. Potsaid, M.F. Kraus, J.J. Liu, D. Huang, J. Hornegger, A.E. Cable, J.S. Duker, J.G. Fujimoto, Total retinal blood flow measurement with ultrahigh speed swept source/Fourier domain OCT. Biomed. Opt. Express **2**(6), 1539–1552 (2011)
53. A.S. Neubauer, L. Reznicek, T. Klein, W. Wieser, C.M. Eigenwillig, B. Biedermann, A. Kampik, R. Huber, Ultra-High-Speed Ultrawide Field Swept Source OCT Reconstructed Fundus Image Quality (ARVO, Fort Lauderdale, USA, 1–5 May, 2011) (Program/Poster # 1327/A264)
54. A. Dubois, K. Grieve, G. Moneron, R. Lecaque, L. Vabre, C. Boccara, Ultrahigh-resolution full-field optical coherence tomography. Appl. Opt. **43**(14), 2874–2883 (2004)
55. A. Dubois, G. Moneron, K. Grieve, A.C. Boccara, Three-dimensional cellular-level imaging using full-field optical coherence tomography. Phys. Med. Biol. **49**(7), 1227–1234 (2004)
56. A. Dubois, J. Moreau, C. Boccara, Spectroscopic ultrahigh-resolution full-field optical coherence microscopy. Opt. Express **16**(21), 17082–17091 (2008)
57. C.K. Hong, Z.Y. Ou, L. Mandel, Measurement of subpicosecond time intervals between two photons by interference. Phys. Rev. Lett. **59**(18), 2044–2046 (1987)
58. A.F. Abouraddy, M.B. Nasr, B.E.A. Saleh, A.V. Sergienko, M.C. Teich, Quantum-optical coherence tomography with dispersion cancellation. Phys. Rev. A **65**(5), 053817 (2002)
59. M.B. Nasr, B.E. Saleh, A.V. Sergienko, M.C. Teich, Demonstration of dispersion-canceled quantum-optical coherence tomography. Phys. Rev. Lett. **91**(8), 083601 (2003)

60. A. Fercher, C. Hitzenberger, M. Sticker, R. Zawadzki, B. Karamata, T. Lasser, Numerical dispersion compensation for partial coherence interferometry and optical coherence tomography. Opt. Express **9**(12), 610–615 (2001)
61. E.D.J. Smith, A.V. Zvyagin, D.D. Sampson, Real-time dispersion compensation in scanning interferometry. Opt. Lett. **27**(22), 1998–2000 (2002)
62. S. Carrasco, J.P. Torres, L. Torner, A. Sergienko, B.E. Saleh, M.C. Teich, Enhancing the axial resolution of quantum optical coherence tomography by chirped quasi-phase matching. Opt. Lett. **29**(20), 2429–2431 (2004)
63. M. Nasr, B. Saleh, A. Sergienko, M. Teich, Dispersion-cancelled and dispersion-sensitive quantum optical coherence tomography. Opt. Express **12**(7), 1353–1362 (2004)
64. M.B. Nasr, D.P. Goode, N. Nguyen, G. Rong, L. Yang, B.M. Reinhard, B.E. Saleh, M.C. Teich, Quantum optical coherence tomography of a biological sample. Opt. Commun. **282**, 1154–1159 (2009)
65. M.C. Teich, B.E.A. Saleh, F.N.C. Wong, J.H. Shapiro, Quantum optical coherence tomography: a review. Quant. Inf. Process (2012, in press), http://people.bu.edu/teich/abstracts/quantum-opt-archive.html
66. M.C. Booth, G. Di Giuseppe, B.E.A. Saleh, A.V. Sergienko, M.C. Teich, Polarization-sensitive quantum-optical coherence tomography. Phys. Rev. A **69**(4), 043815 (2004)
67. M.C. Booth, B.E. Saleh, M.C. Teich, Polarization-sensitive quantum optical coherence tomography: experiment. Opt. Commun. **284**, 2542–2549 (2011)
68. A. Bilenca, T. Lasser, B. Bouma, R.A. Leitgeb, G.J. Tearney, Information limits of optical coherence imaging through scattering media. Photon. J. IEEE **1**(2), 119–127 (2009)
69. R. Bernardes, T. Santos, J. Cunha-Vaz, in *Evaluation of Blood–Retinal Barrier Function from Fourier Domain High-Definition Optical Coherence Tomography*, ed. by O. Dössel, W.C. Schlegel. World Congress on Medical Physics and Biomedical Engineering, vol. 25/11, Munich, Germany, 7–12 September 2009, pp. 316–319 (Springer, Heidelberg, 2009)
70. R. Bernardes, Optical coherence tomography: health information embedded on OCT signal statistics, in *Proceedings of the 33rd Annual International Conference of the IEEE EMBS*, Boston, USA, 30 August–3 September 2011, pp. 6131–6133
71. T. Klein, L. Reznicek, W. Wieser, C.M. Eigenwillig, B. Biedermann, A. Kampik, R. Huber, A.S. Neubauer, *Extraction of Arbitrary OCT Scan Paths from 3D Ultra-High-Speed Ultra Wide-Field Swept Source OCT* (ARVO, Fort Lauderdale, USA, 1–5 May 2011) (Program/Poster # 1328/A265)
72. V.J. Srinivasan, D.C. Adler, Y. Chen, E. Gorczynska, R. Huber, J.S. Duker, J.S. Schuman, J.G. Fujimoto, Ultrahigh-speed optical coherence tomography for three-dimensional and en face imaging of the retina and optic nerve head. Invest. Ophthalmol. Vis. Sci. **49**(11), 5103–5110 (2008)
73. Y. Ikuno, I. Maruko, Y. Yasuno, M. Miura, T. Sekiryu, K. Nishida, T. Iida, Reproducibility of retinal and choroidal thickness measurements in enhanced depth imaging and high-penetration optical coherence tomography. Invest. Ophthalmol. Vis. Sci. **52**(8), 5536–5540 (2011)